

# Ultra-Lightweight Collaborative Mapping for Robot Swarms

V. Niculescu<sup>1\*</sup>, T. Polonelli<sup>1\*</sup>, M. Magno<sup>1</sup>, L. Benini<sup>1,2</sup>

<sup>1</sup>*D-ITET, ETH Zürich, Zürich, Switzerland.*

<sup>2</sup>*DEI, Università degli studi di Bologna, Bologna, Italy.*

**Abstract:** A key requirement in robotics is the ability to simultaneously self-localize and map a previously unknown environment, relying primarily on onboard sensing and computation. Achieving fully onboard accurate simultaneous localization and mapping (SLAM) is feasible for high-end robotic platforms, whereas small and inexpensive robots face challenges due to constrained hardware, therefore frequently resorting to external infrastructure for sensing and computation. The challenge is further exacerbated in swarms of robots, where coordination, scalability, and latency are crucial concerns. This work introduces a decentralized and lightweight collaborative SLAM approach that enables mapping on virtually any robot, even those equipped with low-cost hardware, including miniaturized insect-size devices. Moreover, the proposed solution supports large swarm formations with the capability to coordinate hundreds of agents. To substantiate our claims, we have successfully implemented collaborative SLAM on centimeter-size drones weighing only 46 grams. Remarkably, we achieve results comparable to high-end state-of-the-art solutions while reducing the cost, memory, and computation requirements by two orders of magnitude. Our approach is innovative in three main aspects. First, it enables onboard infrastructure-less collaborative mapping with a lightweight and cost-effective solution in terms of sensing and computation. Second, we optimize the data traffic within the swarm to support hundreds of cooperative agents using standard wireless protocols such as ultra-wideband (UWB), Bluetooth, or WiFi. Last, we implement a distributed swarm coordination policy to decrease mapping latency and enhance accuracy.

## INTRODUCTION

Nowadays, swarms of autonomous robots find applications in many sectors, from industry to civil markets, including biomedical and healthcare (1, 2). Key tasks such as perception or mapping can be carried out more effectively and at lower latency by a swarm than by a single agent (3). However, the design of a collaboration scheme between the agents of a swarm is still an unsolved challenge in many robotics applications (2). The core principle of swarm coordination relies on a set of shared rules based on local-global sensory inputs and communication with neighboring agents. In addition, not relying on centralized processing is crucial for increasing robustness, ensuring that the failure of a single robot does not compromise the entire mission execution (2, 4, 5). Moreover, achieving autonomous and coordinated robot navigation in real-world environments poses significant scalability challenges in designing a shared coordination scheme that is feasible for hundreds of cooperative agents (6).

Aerial light shows featuring hundreds of quadcopters and the concept of highly automated warehouses predominantly relying on robotic sorters underscore the current technological landscape (7–9). However, those systems mostly follow preprogrammed trajectories calculated on a base station (10), often relying on external infrastructure for computation, localization, and communication (6, 11). Navigation and cooperation of a swarm of robots in unexplored and GNSS-denied environments, without the support of any external framework, remains an open research challenge (2, 12). In particular, the design of an efficient and robust infrastructure-free and decentralized solution for agile collaborative robots, supporting navigation, distributed sensing, and mapping is a challenging research goal in the robotics field (3, 13–15). The ongoing industrial and

social revolution is driving the deployment of robots in everyday life, beyond heavily controlled environments, such as automated production lines (16). Therefore, heterogeneous and cost-effective robotic platforms will soon need to operate in a variety of environments, often uncontrolled, in proximity to humans, animals, and within residential spaces (1, 2). In this context, enabling the use of robots across various applications, reducing the hardware costs associated with sensing and computation, is crucial (17). Undoubtedly, the current societal viewpoint of autonomous and intelligent machines as exclusive and costly needs to shift towards seeing them as accessible, plug-and-play, and cost-effective tools (18). Moreover, in the context of specific application scenarios, such as space exploration and first-aid, hundreds of droids will be deployed in unexplored and infrastructure-less scenarios without the possibility of human intervention (1), pushing even more the need for lightweight, cost-effective, and distributed solutions for autonomous and heterogeneous swarms of miniaturized robots (19, 20).

Multi-robot distributed simultaneous localization and mapping (SLAM), in which a group of autonomous agents jointly create and maintain a shared map of the surroundings, is one of the essential elements to enable distributed cooperation and optimal task planning (5, 20, 21). Typical SLAM methods produce high-resolution 3D maps, exploiting vision-based solutions based on stereo cameras or light detection and ranging (LiDAR) depth sensors. However, these standard approaches are generally very demanding in terms of computational and memory resources, requiring expensive system-on-module (SoM) platforms integrating CPUs and GPUs with several gigabytes of local memory (22, 23). Other limitations include the system cost of the hardware, sensing, and the wireless bandwidth required to exchange real-time information with other agents in the swarm. State-of-the-art (SoA) dense vision-based SLAM (vSLAM) approaches require the transfer of up to 3.5 GB of data in a centralized scheme, or ~150 MB per robot in a distributed and communication-efficient scheme (14, 24). Therefore, an increased number of robots would saturate a WiFi network with only a few agents, in the range between 3 and 10, generating a fundamental scalability bottleneck (14, 24). Overall, there has yet to be a fully distributed and highly scalable SLAM system addressing all the associated challenges of supporting large numbers of collaborative agents operating with limited onboard resources without relying on an external infrastructure for sensing and/or computation. These challenges encompass communication and computational requirements alongside the hardware costs for sensing and data processing (20).

This work approaches the research challenge of collaborative SLAM (C-SLAM) with a novel approach, in all its terms, from sensing to computation, in challenging real-world environments such as indoor areas filled with obstacles. The primary contribution is a fully distributed C-SLAM system for multi-robot dense mapping using sparse sensing. Our system enables a swarm of collaborative robots to estimate a 2D mesh model of the environment in real-time. Each agent runs entirely onboard the SLAM algorithm to process depth-inertial sensor data based on local state estimation and a low-power, cost-effective, and lightweight 64-pixel depth camera. Wireless communication can be supported by any commercial standard, including WiFi and Bluetooth low energy (BLE) (25), while for the scope of this work we employ ultra-wideband (UWB) to also enable infrastructure-less intra-swarm ranging (i.e., distance estimation). A fully distributed localization and ranging procedure is triggered to perform inter-robot collision avoidance and place recognition. Each swarm agent performs real-time local mesh updates to correct mapping drift through multi-robot loop closure using the Iterative Closest Point (ICP) algorithm (26), enhancing both local accuracy and global map consistency. Moreover, the proposed implementation is modular, allowing different agents to join/leave the swarm dynamically, supporting flexible and heterogeneous teams of robots.

While LiDARs paired with depth-based SLAM prove to yield high mapping accuracy, they have a high associated cost of a few hundred dollars. Thus, mounting such a unit onboard every robot in a swarm would dramatically increase the total cost. We demonstrate the possibility of enabling mapping with similar SoA accuracy using \$5 time-of-flight (ToF)  $8 \times 8$  multizone depth sensors and a low-power commercial-off-the-shelf (COTS) microcontroller. So far, SLAM, and especially C-SLAM, has been a prerogative for high-end platforms featuring GPUs coupled with several gigabytes of memory that cost hundreds of dollars. On the other hand, our highly optimized C-SLAM pipeline can run in real-time on COTS ultra-low-power microcontrollers featuring 1.5 MB of RAM. With a power budget of  $\sim 100$  mW and a cost below \$10, our C-SLAM engine can optimize the map in about 250 ms after every loop closure. The required power budget, including sensing and computation, is below 1 W. Therefore, our work provides mapping capabilities to a wide range of robotic platforms, including inexpensive, lightweight, and resource-constrained drones.

In addition to the theoretical formulation and simulation-based studies, our work demonstrates with practical and extensive field experiments how a team of ultra-constrained centimeter-size unmanned aerial vehicles (UAVs) can collaboratively map a generic environment relying only on onboard capabilities for mapping, communication, localization, and sensing. Fig. 1 displays multiple views of our swarm of nano-UAVs (19) deployed in-field, performing collaborative mapping of an indoor environment. Our contributions can be summarized as follows: (i) a distributed lightweight C-SLAM framework that runs onboard and performs depth-based loop closure and distributed trajectory optimization. (ii) A communication scheme that enables the robots to coordinate and minimizes the amount of exchanged data. (iii) A navigation strategy that attempts to uniformly distribute the swarm in an unexplored environment. While our experimental evaluation is performed with UAVs, our C-SLAM system can be deployed on any robot that can accommodate a payload of approximately 10 g, a power budget of 1 W, and that is equipped with odometry capabilities. Note that the odometry capabilities can even be achieved using low-cost and low-resolution sensors (27), such as the PMW3901 camera that features a resolution of  $35 \times 35$  pixels. These sensors do not need to provide high accuracy, as the odometry errors are corrected by the C-SLAM algorithm.

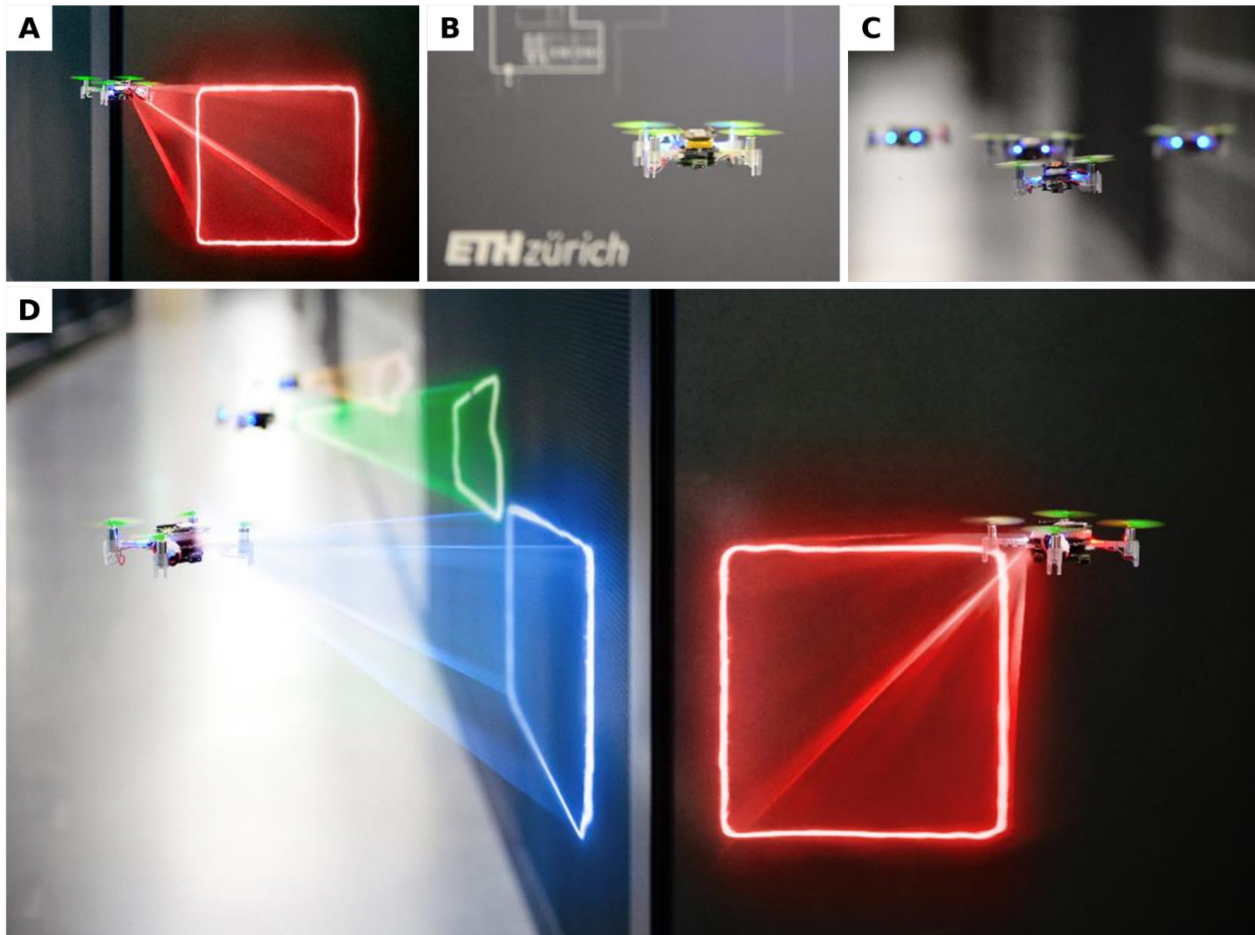


**Fig. 1. Illustrations of a swarm of miniaturized UAVs using our SLAM system to map a real environment.** (A) A miniaturized UAV (46 g) with a size of 10 cm, equipped with four VL53L5CX ToF 8×8 multizone depth sensors, mapping a wall. (B) Overview of the miniaturized UAV including sensing, communications and ranging via UWB, and onboard computing with a COTS microcontroller. (C) Swarm formation in a real deployment. (D) Four cooperative miniaturized UAVs mapping a real environment without any external support for localization and computation.

## **RESULTS**

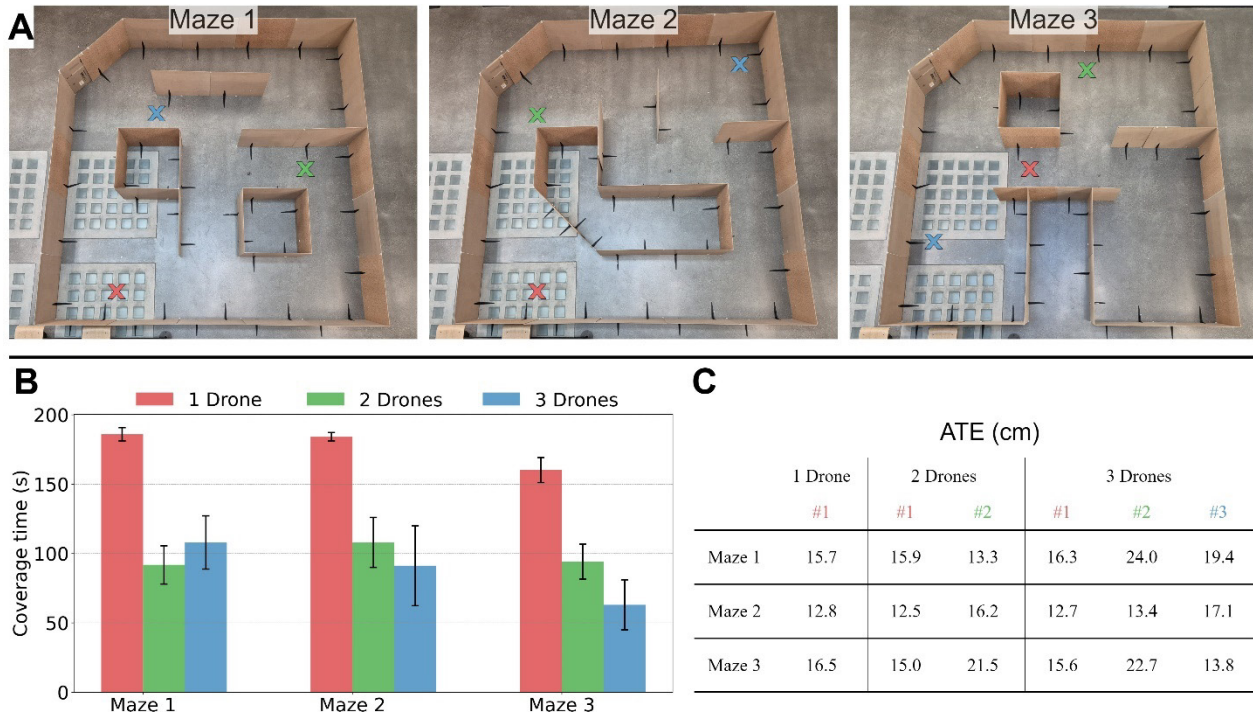
We demonstrate the efficacy of our system by conducting practical field experiments within both controlled and realistic environments, encompassing general indoor areas. Moreover, C-SLAM is compared with SoA recent works in terms of accuracy and scalability, demonstrating how hundreds of robotic agents can collaborate, sharing data and scans over standard wireless protocols. Within the scope of our mapping mission, a variable number of drones, between one and four, explore different environments, employing our exploration and C-SLAM algorithms. Furthermore, a scalability test varying the swarm size between 2 and 200 agents has been conducted in a separate experiment. During flight, drones utilize UWB radio communication to convey their respective positions to one another, as well as the distances between them. The exploration strategy is designed to efficiently cover the entire environment, facilitating loop closure. When a drone is found in an intersection, it steers toward the direction with fewer robots to achieve an even robot distribution, increasing the area coverage rate. When two drones encounter one another head-on, they execute a 180° turn and continue exploring to prevent collisions. Throughout the mission, our C-SLAM algorithm running onboard each drone corrects the trajectory drift by comparing scenes of the environment associated with revisited places (i.e., loop closure). We distinguish two types of loop closures: (i) intra-drone loop closures, occurring when the same drone captures the revisited scenes, and (ii) inter-drone loop closures, occurring when two or multiple different drones capture the

scenes. The intra and inter-drone loop closures are essential for ensuring the accuracy of the local-global maps and for maintaining overall consistency on the reference frame. Our evaluation is centered on assessing how the coverage time scales with the number of drones, the absolute trajectory error (ATE) of each drone within the swarm, and the mapping accuracy of the collective global map.

### Experiments in a controlled environment

First, we evaluate our system in a controlled environment consisting of mazes built out of chipboard panels of  $0.8 \text{ m} \times 1 \text{ m}$ . The goal is to evaluate the coverage time and mapping accuracy, observing how these metrics are influenced by varying the number of drones. To demonstrate the adaptability of our system to different spatial configurations, we evaluated its mapping efficacy across several mazes with distinct geometries. The Vicon Vero 2.2 motion capture system installed in our testing arena provides the ground truth for the evaluation. Fig. 2A illustrates the three distinct mazes subjected to this analysis, with the take-off positions of the drones marked by an “x” of three distinct colors. After take-off, the drones embark on their exploration and mapping tasks, propelled by the underlying exploration algorithm. For each configuration, Fig. 2B shows the time the drones require to cover all accessible areas within the maze. As anticipated, the longest duration correlates with the experiments utilizing a single drone. Moreover, introducing a second drone yields a significant reduction in coverage time by 48%, 43%, and 41% for Maze 1, Maze 2, and Maze 3, respectively. However, transitioning to a configuration with three drones does not yield a proportional decrease in coverage time; reductions are observed at only 50% and 60% for Maze 2 and Maze 3, respectively, when compared to the single-drone setup. This suggests a saturation trend when increasing the number of agents per square meter. For Maze 1, the coverage time increases by 18% compared to the two-drones experiment. This phenomenon can be attributed to the drones intersecting paths twice in Maze 1, as opposed to once and not at all in Mazes 2 and 3, respectively. Since intersections compel the drones to reverse direction and retrace their previously covered path, they increase the coverage time. This highlights the importance of adjusting the drone count based on the size of the explorable area.

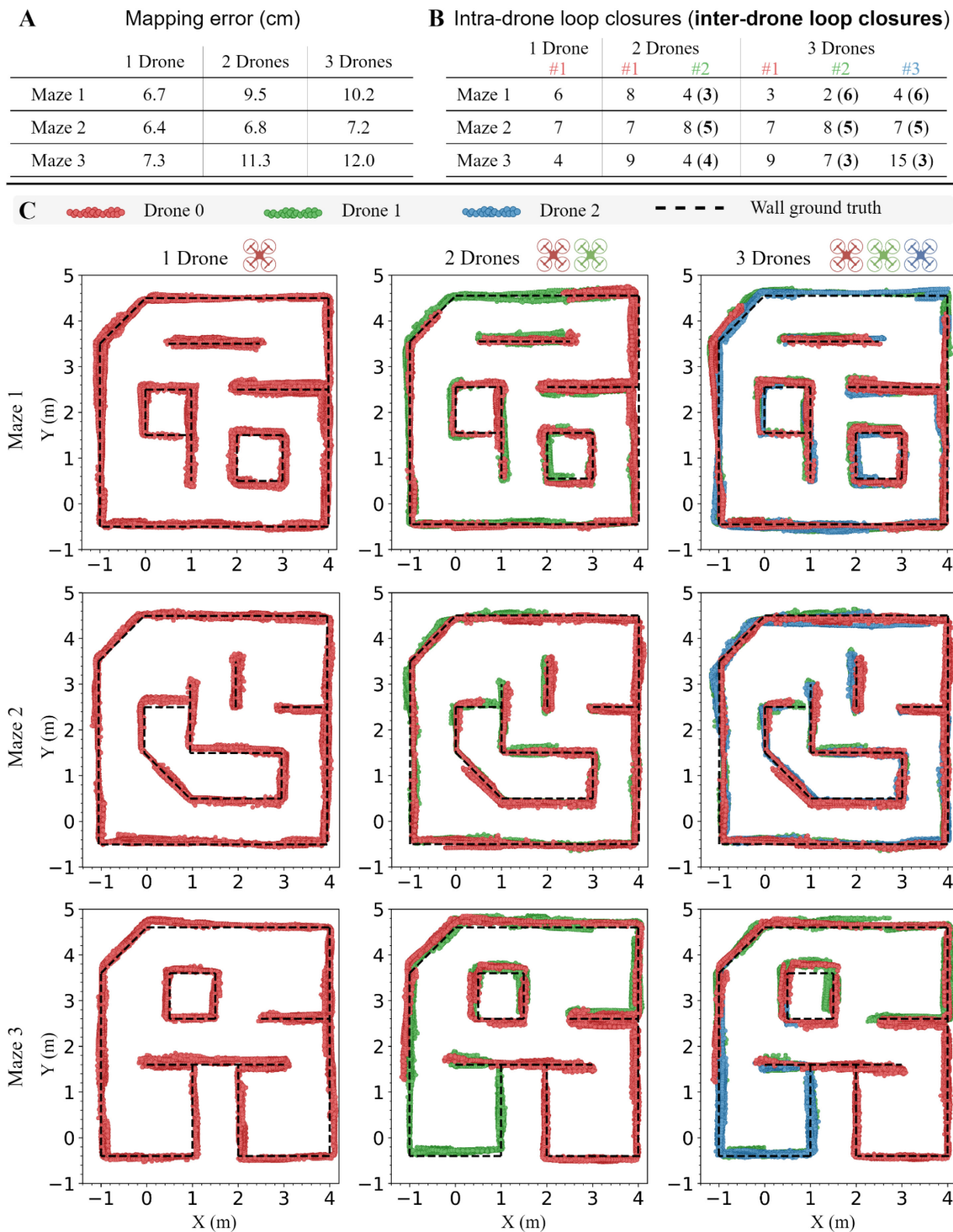
The table in Fig 2C shows the ATE for each configuration, which varies in the range of 12.5 cm – 24 cm, with the highest values for the configuration of Maze 1 and three drones. Given that rotational movements worsen the ATE, due to yaw angle observability limitations of nano-UAVs operating indoors, and each encounter between drones necessitates a  $180^\circ$  spin, it logically follows those configurations characterized by a higher frequency of intersections exhibit increased ATE values. Furthermore, Maze 3 also shows a relatively high ATE, regardless of the number of drones. In this case, it is not the drone intersection that increases the ATE but the geometry of the maze, as the two “rooms” at the bottom are only connected through an upper path. The absence of loop closures in the lower section of Maze 3 results in distortion of the trajectory, thereby influencing the ATE. Within the scope of this work, we specifically selected a constrained drone platform featuring limited odometry capabilities that restrict the trajectory estimation accuracy to demonstrate how C-SLAM provides stability and robustness even under poor observability conditions.



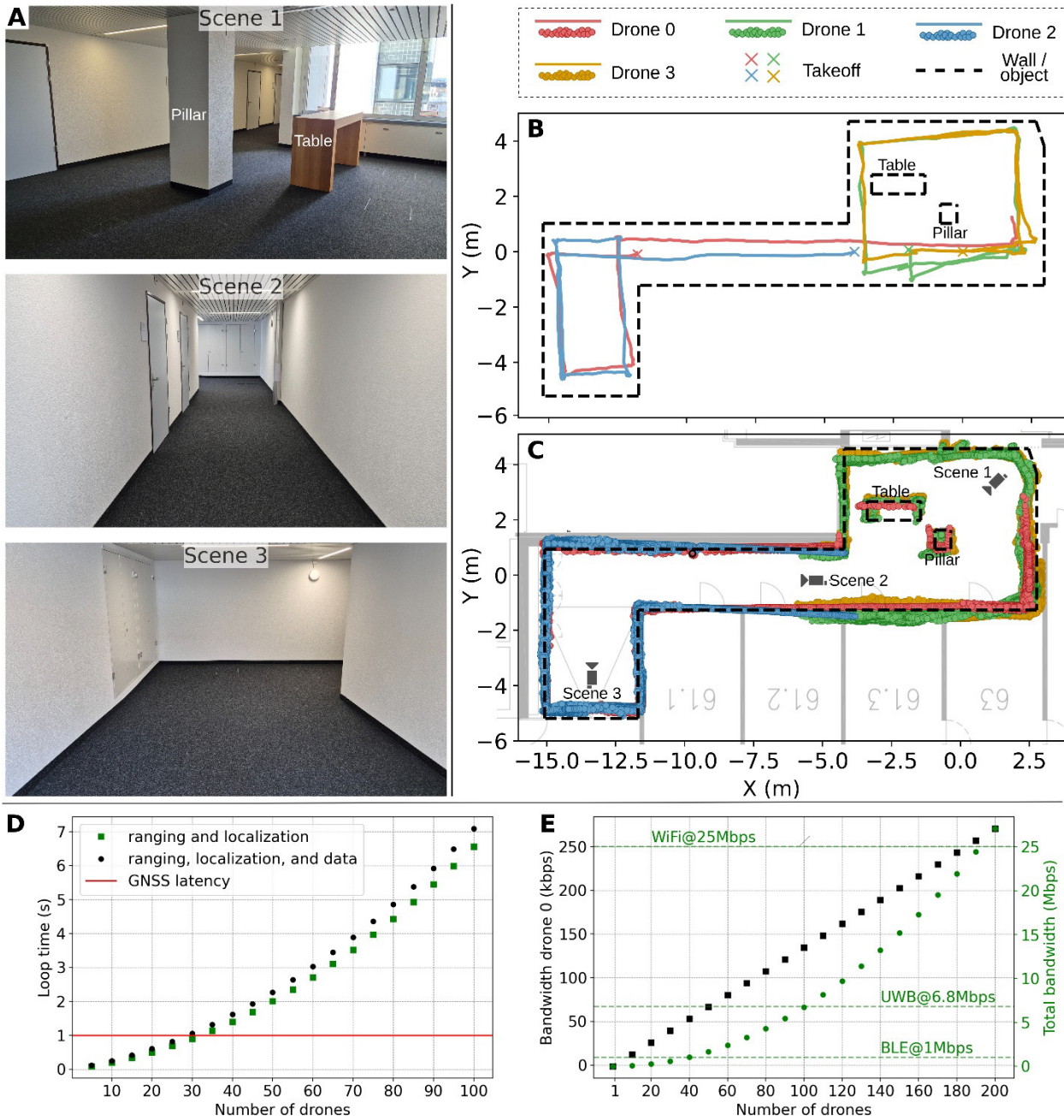
**Fig. 2. Environment overview and exploration performance.** A top-view photographic collage of the mazes employed in the mapping evaluation is illustrated in (A). The coverage time results for one, two, and three drones in each maze are shown in (B), illustrating the efficiency of collaborative exploration. (C) provides an analysis of the absolute tracking error (ATE) for each robot within the swarm, highlighting the precision of navigation across all configurations.

Fig. 3 presents the mapping outcomes for each maze aimed at evaluating the effect of multiple inter-drone loop closures on the map’s integrity. The metric used to assess the overall C-SLAM accuracy is the absolute mapping error. This metric first calculates the projection to the closest straight line (or its extension) for every point in the map. Then, the mapping error in Fig 3A is computed as the root-mean-squared-error (RMSE) of all the projections. RMSE does not only depend on the state estimation error, but it also correlates with the shape of the environment and the measurement noise of the depth measurements. The overall swarm mapping error spans from 6.4 cm to 12 cm, as shown in Fig. 3A. The results are aligned with Fig. 2C, yielding the smallest overall mapping error for Maze 2, and the largest error for Maze 3. This is expected because each drone has its own biases, and anchoring the maps in a finite number of points may not completely align them. Fig. 3B shows how many loop closures are performed in each mission. While the numbers are comparable among configurations, we notice a larger amount of intra-drone loop closures when mapping Maze 3 with three drones. This is due to the nature of the exploration policy, as once a drone reaches one of the bottom “rooms” of Maze 3, it is likely to perform several loops until it exits the area. This leads to multiple intra-drone loop closures performed in a short time. The maps presented in Fig. 3C underwent a filtering phase, where points with a low density of neighbors were removed, assuming they likely represent outliers corresponding to nearby drones rather than real objects. This approach enhances the map’s accuracy by ensuring it reflects only points associated with physical features, based on the premise that genuine features are typically surrounded by a cluster of points.





**Fig. 3. Mapping results in a controlled environment.** The mapping error results for one, two, and three drones in each maze are provided in (A), while (B) indicates how many loop closures were performed in each experiment. (C) shows the maps produced at the end of the mission in each maze, illustrating how the individual maps are aligned and merged by our C-SLAM algorithm.



**Fig. 4. Real-world results.** (A) A trio of photographs representing samples from the real environment where the mapping mission is conducted, highlighting the encountered obstacles. The trajectories of each drone are depicted in (B), with each trajectory color-coded according to the legend for clear differentiation. The collaborative map created by the drone swarm is displayed in (C), which also indicates the locations where the three photos presented in (A) were taken. The swarm scalability results are proposed in (D) and (E), comparing the wireless transmission and localization latency against the swarm size. In (E), the loop time of our setup is depicted, including UWB ranging and localization alone and with the effect of transferring scans. Our infrastructure-less setup reaches a latency comparable to GNSS-based systems with 30 swarm agents. (E) shows the radio bandwidth per drone (drone 0 has the highest bandwidth) and for the whole swarm, highlighting the nominal data rate of common wireless communication technologies.

### Experiments in a real-world office environment

We also prove the effectiveness of our C-SLAM in a realistic environment. For this purpose, we map an  $18\text{ m} \times 10\text{ m}$  area in an office environment employing a swarm of four nano-UAVs, depicted in Fig. 7. The number of drones was estimated from the results in Fig. 2B, where coverage time saturation implies an optimal number of agents per square meter. Moreover, the experiment setup is comparable with recent collaborative mapping papers (14). Three scenes of the



environment are illustrated in Fig. 4A, while the obstacles are labeled in Scene 1. This environment is selected as the worst-case scenario, with few favorable areas for loop closure and a thick concrete wall affecting wireless communication. The proposed experimental setup pushes the limits of C-SLAM, enabling distributed mapping on ultra-constrained nano-robotic platforms with limited observability.

Since there is no trajectory ground truth in this experiment, we represent in Fig. 4B the onboard estimated trajectories that were corrected by the C-SLAM algorithm to show the effectiveness of our exploration algorithm in distributing the drones through the whole environment. They initiate their flight from positions denoted by 'x', achieving complete area coverage in approximately 60 s. Fig. 4C shows how the map looks at the end of the mission, where the data points produced by each drone are represented with a distinct color. Additionally, the locations where each of the three environmental snapshots were captured are indicated. Notably, the experiment exhibits accurate corner alignment attributed to inter-drone loop closures. The most significant discrepancy is noted adjacent to the longest wall at the bottom of the area, approximately 15 m, where the absence of loop closures over extended distances results in substantial accumulated trajectory drift, thereby inducing ATE errors that are not fully rectifiable. Conclusively, the experiment leads to a mapping error of 29.7 cm. It is important to note that, in contrast to the maze-based experiments characterized by a more confined area, in this experiment, the drones frequently encountered UWB radio out-of-range situations limiting the relative intra-swarm localization, predominantly due to the obstructions of concrete walls found in the line of sight. Despite these challenges, our system demonstrated robustness against connection-drop conditions, and it consistently demonstrated the ability to recover from such states when the drones returned within the communication range.

## DISCUSSION

So far, accurate collaborative SLAM mapping has been a prerogative of powerful and expensive robotic platforms such as GPUs-based ones, limiting swarm formations to few units due to the high volume of exchanged data necessary for loop closure and map alignment (3). Moreover, the majority of existing SLAM systems rely on external infrastructure support for localization and computation (9, 22), such as GNSS or motion capture systems. Recent SoA works on onboard and decentralized solutions mainly focus on maximizing the mapping accuracy but do not address latency and scalability (4, 28). Despite relying on high-end platforms, recent works reach an average global map update in the range between 0.1 s to 7 s (22, 29). Moreover, such a large data volume bounds the minimum latency, which in some cases reaches up to 5 s due to computation and data transmission overhead (24). Despite these powerful computational platforms, more similar to a server than an embedded system, the CPU load level reaches a mean of 93% (24) or half of the total load for autonomous car competitions (23) only to perform 2D mapping. Under these circumstances, SoA works on distributed and collaborative SLAM (14) feature a mapping error in the range of 20 to 25 cm for indoor operation. We achieved a comparable error of about 30 cm, but our system requires less than 1.5 MB of RAM and a sensor setup that costs about \$20. Note that the majority of this error comes from the lack of onboard odometry performance of our miniaturized and cheap robotic platform, featuring an ATE up to 24 cm; hence the C-SLAM system performs similarly to the SoA in an equivalent setup. To further affirm the existing constraints in computation and communication, high-speed autonomous racing quadcopters are unable to execute SLAM algorithms in real-time (30), mapping the environment in a preliminary calibration phase with the aid of external infrastructure.

Our system prioritizes scalability, hardware cost, and computational load. A scalability study, based on the intra-swarm data communication and localization, is presented in Fig. 4D and Fig. 4E, demonstrating the possibility of supporting up to 200 robots. We define loop time as the total time necessary for the drones in the swarm to communicate their positions to each other, the distances between them, and the scans. In the communication scheme we propose, only one drone

transmits at a time, and the transmission scheduling for each drone occurs in increasing order based on its ID. Therefore, a large loop time would impact the update rate of the positions, decreasing the robustness of collision avoidance. Fig. 4D shows how the loop time depends on the number of drones. The position and distance updates are relevant for inter-drone collision avoidance, while the scan transfer is associated with mapping and loop closure. Consequently, Fig. 4D illustrates the loop time with and without considering the influence of the scans. Given that the scan acquisition frequency is usually considerably lower than the loop frequency, this study presumes that each drone sends at most one scan per loop and no more than 20% of the drones in the swarm send a scan within the same loop. We highlight that a latency comparable to GNSS-based localization is obtained for a swarm size of 30 drones. Moreover, while previous works (24) achieve a 2.7 s latency with a swarm of 10 drones (data transmission only), our system allows a swarm of 55 robots with the same latency (data transmission and localization).

We highlight that the loop time in Fig. 4D mainly depends on transmitting the drones' positions and distances. However, combining an absolute positioning system with our C-SLAM pipeline would alleviate the need to wirelessly measure the relative drone positions. In such a scenario, the only scalability limitation would lie in the necessary bandwidth for transferring the scans. Fig. 5E shows the bandwidth requirement as a function of the number of drones. Furthermore, we represent both the total swarm bandwidth and the bandwidth required by drone 0 (i.e., the worst case). In addition, the figure shows that conventional communication technologies (25) such as WiFi, UWB, and BLE can accommodate about 190, 100, and 40 drones, respectively. Although the WiFi protocol (Wi-Fi 6 - IEEE 802.11ax) can reach up to 600 Mbps, in line with the scope of this work, we selected a cheap and miniaturized WiFi module (NINA-W10 from u-blox) supporting up to 25 Mbps. Within this investigation, we consider an average number of five scans per minute and a scan size of 2 kB. The possibility of pairing our setup with BLE enables even teams of insect-size robots to collaboratively map a previously unknown environment (17).

Our C-SLAM solution relies on graph-based SLAM (29) and distributes the computational load to all mapping agents in the swarm. The pose graph each drone stores and optimizes depends on how long it traveled (i.e., internal poses), and a new external pose is added whenever an inter-drone loop closure occurs. Thus, the graph size depends on the size of the environment and its geometry - paired with how many loop closures arise. For example, an environment where a robot acquires 1400 poses and performs five loop closures results in  $\sim 250$  ms execution time onboard a 100 mW microcontroller. The largest graph an individual drone can optimize with this hardware setup has about 3000 poses, corresponding to an environment of about 400 m<sup>2</sup>. Due to the distributed nature of our C-SLAM solution, this area scales about linearly with the number of robots.

Although the ToF sensors we employ in this work are lightweight, energy-efficient, and cost-effective, conventional LiDARs maintain superiority in terms of accuracy. Primarily, LiDARs commonly feature an extended operational range, facilitating the mapping of distant environmental regions. Conversely, our ToF depth sensor is constrained by a maximum range of 4 m. Moreover, LiDARs frequently boast superior angular resolution, leading to measurement precision that is less dependent on distance magnitude, allowing for higher accuracy scans and scan-matching. However, to precisely quantify the differences in mapping accuracy, we map again the environment from Figure 4A using a ground legged robot equipped with a Hokuyo UTM-30LX-EW LiDAR. This experiment results in a mapping error of about 10 cm, which is in the same order of magnitude as the error obtained with our system (i.e.,  $\sim 30$  cm). However, our system's odometry features an error of up to 24 cm, while the ground legged robot features a sub-centimeter odometry error. Therefore, our C-SLAM guarantees map consistency and stability also in the presence of limited odometry accuracy, typical of low-cost or miniaturized robotic platforms. Moreover, such a LiDAR costs

about 100 times more than our sensor setup, and the computing platforms onboard the ground robot (i.e., Intel NUC and Nvidia TX2) cost 100 times more than the SoCs we employ.

The C-SLAM pipeline we propose in this manuscript supports only 2D mapping, an optimal tradeoff between mapping accuracy and memory footprint. Yet, the raw depth measurements from the ToF sensors are acquired in matrix form. While our 2D approach reduces the measurements from matrix to row format, a 3D map can be obtained by projecting all matrix measurements in the world frame. Within our experiments, the drones are aware of their initial take-off locations and continue keeping track of them during the mapping mission. While the initial robot locations might not be known in all real-world applications (e.g., random deployment), our work focuses on the collaboration between drones and maintaining the consistency of the global map over time. To address the initial localization problem, our system can be paired with one of the previous works addressing this issue. For example, the authors in (31) propose a relative localization algorithm based on pair-wise UWB range measurements.

## MATERIALS AND METHODS

In this section, we discuss the details of the ultra-lightweight C-SLAM and the exploration strategy implemented in our field tests to improve the mapping coverage in unknown environments. Furthermore, we expound upon the C-SLAM scheme and the mechanism used by each swarm agent to rectify its trajectory and align maps to ensure global consistency. Lastly, we describe the hardware architecture and how it can be replicated.

### Collaborative SLAM scheme

Our mapping system employs graph-based SLAM, which represents the robot trajectory as a pose graph. The nodes are poses sampled at discrete times ( $\mathbf{x}_k$ ) and the edges are relative measurements between the poses. Each  $\mathbf{x}_k = (x_k, y_k, \varphi_k)$  is expressed in the world frame and consists of the 2D position and heading, where  $k$  represents the timestamp. Furthermore, we note as  $\mathbf{z}_{ij}$  the relative measurement from poses  $i$  to  $j$ . Any two consecutive nodes within the graph of a robot are connected by an edge characterized by the 3-element vector  $\mathbf{z}_{i,i+1}$  provided by the drone’s state estimator -- named odometry edge. At every instant  $k$ , the robot not only stores a new pose but also acquires 32 distance measurements from the four depth sensors, which constitute a depth frame. The poses and their associated depth frames (i.e., sparse measurements) are sufficient to produce the map by projecting the distance measurements in the world frame (dense mapping). However, the odometry edges are affected by errors, and computing the pose values using forward integration would cause the trajectory to drift over time. Consequently, our C-SLAM uses a correction mechanism that compares observations of the environment in revisited locations. These observations are tiny map tiles generated out of 20 consecutive depth frames, named scans. Fig. 6A shows how a scan is created while appending projected depth frames. Because the cumulative FoV of the four depth sensors is  $180^\circ$ , the drone also spins in place by at least  $45^\circ$  to achieve full coverage during the scan acquisition. Each scan is matched with a pose, representing the robot position right before the acquisition starts. Using scan-matching, our system determines the optimal rotation and translation that overlaps one scan over the other. Since the poses and their associated scans are acquired at the same time, the transformation resulting from scan-matching also applies to the poses. In this way, when the drone revisits a location, scan-matching determines an accurate rigid body transformation relative to a pose that was previously acquired in that location. This transformation is incorporated in the graph as an additional loop closure edge. Then, our system uses pose-graph optimization (PGO) (29), propagating the loop closure information through the whole graph to correct all previously acquired poses. In our work, we employ the ICP algorithm to perform scan-matching (26).

The scan matching mechanism facilitates not only the correction of a robot's pose in relation to its own previous pose (i.e., intra-drone loop closure) but also in relation to the pose of another drone (i.e., inter-drone loop closure). This is achieved by aligning overlapping scans from different drones to perform inter-drone loop closure. Fig. 6B shows the graphs associated with multiple agents, where each agent maps a different environmental area. Nonetheless, an overlapping segment is necessary to establish connections between the drones' respective graphs. Within our distributed optimization scheme, each agent exclusively engages in inter-loop closures with drones possessing lower IDs. Furthermore, the graph each drone optimizes consists of its own poses alongside the external poses. To ensure coherence across all graphs, external poses remain unaltered during PGO, serving solely as reference points (i.e., anchor points) for optimizing self poses. In other words, each drone aligns its map relative to the drones possessing lower IDs.

$$X^* = \underset{X}{\operatorname{argmin}} \left( \underbrace{\sum_i \mathbf{e}_{i,i+1}^T \Omega_{odom} \mathbf{e}_{i,i+1}}_{\text{odometry edges}} + \underbrace{\sum_{i,j} \mathbf{e}_{i,j}^T \Omega_{LC} \mathbf{e}_{i,j}}_{\text{intra LC edges}} + \underbrace{\sum_{i,k} \mathbf{e}_{i,k}^T \Omega_{LC} \mathbf{e}_{i,k}}_{\text{inter LC edges}} \right) \quad (1)$$

Equation 1 shows the optimization problem of the distributed PGO, which is solved onboard by each agent. Let  $X = \{\mathbf{x}_0, \mathbf{x}_1, \dots\}$  be the set of all poses in the graph. We note as  $\hat{\mathbf{z}}_{i,j}$  the prediction of an edge measurement, which is the edge measurement computed out of two poses  $\mathbf{x}_i$  and  $\mathbf{x}_j$ . Therefore, solving the problem in Equation 1 reduces to determining the pose values that ensure consistency between the edge measurements  $\mathbf{z}_{i,j}$  and the predicted measurements  $\hat{\mathbf{z}}_{i,j}$ . The maximum likelihood solution associated with Equation 1 is equivalent to minimizing the sum of squared differences  $\mathbf{e}_{ij} = \mathbf{z}_{i,j} - \hat{\mathbf{z}}_{i,j}$ . Each term  $\mathbf{e}_{ij}$  is paired with an edge and weighted by a diagonal information matrix  $\Omega$ . When computing the errors associated with the odometry edges,  $j = i + 1$  as the odometry edges are always connecting consecutive poses. Moreover, the external poses  $\mathbf{x}_k$  used to compute the inter-drone loop closure edges remain unchanged during the optimization.

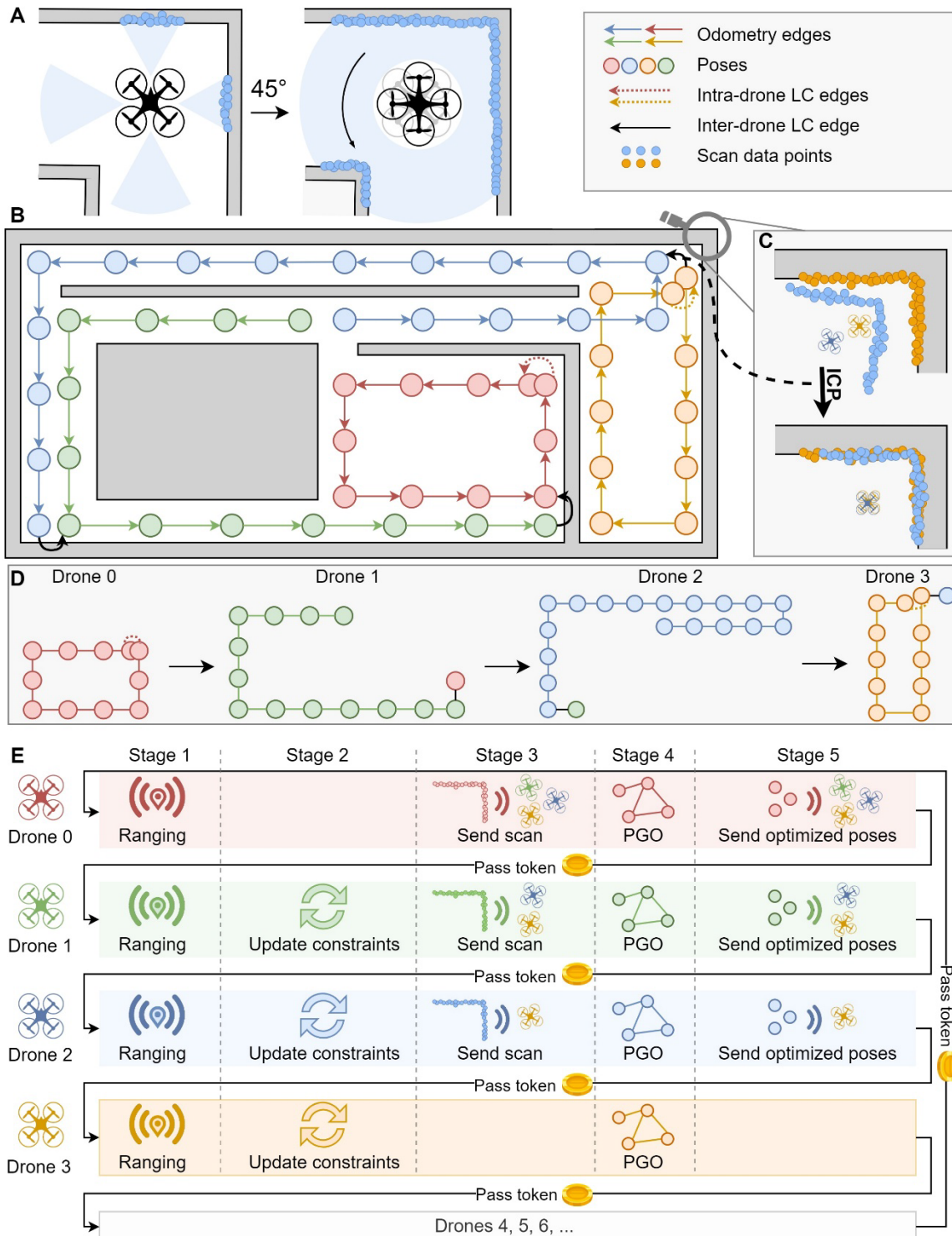


**Fig. 6. The CSLAM scheme.** (A) Illustration of how a drone acquires a scan once reaching a texture-rich location. (B) Composite visualization of individual pose graphs and how they are connected through inter-drone loop closure edges. (C) Illustration on how ICP determines the relative transformation between two poses by overlapping their associated scans. (D) Representation of the cascaded distributed SLAM optimization, illustrating the graph optimized by each drone. (E) The robust communication protocol. It supports a variable number of swarm agents while minimizing data traffic.

### Communication and ranging protocol

The exploration algorithm requires knowledge of the relative positions and distances to all the other swarm agents. Furthermore, the C-SLAM scheme requires scans from the other drones to perform



inter-drone loop closures. Fig. 6E shows the multi-stage communication protocol that orchestrates how the drones exchange information. The protocol is implemented using UWB for the scope of this work, which is used for both data transmission and ranging. However, it can be implemented leveraging alternative commercial standards, such as WiFi and BLE (25). Moreover, the protocol is token-based, implying that only one drone can transmit at a time, avoiding packet collision effects and, consequently, decreasing wireless traffic. After a drone receives the token, it first performs ranging with all drones of higher ID. We employ the double-sided two-way-ranging (IEEE 802.15.4a-2007) for ranging (3, 32), which involves a pairwise point-to-point distance estimation. Furthermore, the drones also embed their relative positions (obtained from the state estimator) in the ranging messages. After drone  $i$  completes Stage 1, it is aware of all distances and positions of the drones with ID  $i+1$  or higher.

In Stage 2, a drone verifies if it has any received external scans in the buffer. Then, it pairs each external scan with the internal scan acquired at a distance smaller than  $D_{th}$ . If multiple internal scans meet this condition for a given external scan, the system chooses the one acquired the earliest. For each pair, it runs ICP and derives a new inter-drone loop closure edge. In Stage 3, the drone checks if a new scan has been acquired since the last time it had the token, and if this is the case, it broadcasts the scan to all drones with higher IDs. The other drones store the received scan in a buffer and process it during Stage 2 the next time they acquire the token. Stage 4 consists of optimizing the pose graph. This is always initialized by drone 0 when it completes a certain number of loop closures or periodically at a defined time interval. To initiate the cascaded PGO, drone 0 sends an extra message to drone 1 along with the token handoff. Subsequently, each drone mirrors this action, relaying the message forward in sync with the token's progression to notify all drones to perform PGO during their next turn.

Until now, the formation of inter-drone loop closure edges through transformations between scans from different drones has been explored. We have established that all external scan positions serve as reference points in the PGO process. Nonetheless, when a drone updates its pose graph, the positions change, meaning that the loop closure edges based on that drone's previous scan positions become out-of-date. Since sending the whole updated scan based on the new pose values would be inefficient, we derive a way of updating an inter-drone loop closure edge only based on the previous edge value and the new pose. Consequently, whenever a drone performs PGO, it also sends the new values of the scan poses to the other drones with higher IDs – performed within Stage 5. The size of the updated poses (i.e., 12 B per pose) is negligible compared to the scan size.

We mention that while the communication protocol iterates continuously through the drones in the swarm, it is only Stage 1 which is executed every time the drone acquires the token. An arbitrary drone  $i$  requires  $N - i - 1$  distance measurements in Stage 1 to communicate with all higher ID drones, where  $N$  is the total number of drones. This results in a total of at most  $N(N - 1)/2$  communications within a whole round, where each ranging requires about 4 ms. Stage 2 is typically performed several times per minute, depending on how often external scans are received and, therefore, how many texture-rich locations are in the environment. The time spent in this stage depends quasi-linearly on the number of drones, see Fig. 4D, and it is dominated by the execution time of ICP (typically below 20 ms per scan-matching). Since PGO does not need to happen too frequently, Stages 4 and 5 are typically executed once per minute in a normal indoor scenario.

The designed system exhibits robust fail-safe characteristics, capable of addressing radio disruptions, hardware malfunctions, or temporary absence of swarm agents. All data messages are acknowledged, and in the event of a missing response, retransmission is tried up to three times. In instances where a drone, designated by ID  $i$ , attempts to pass the token to drone  $i + 1$  without

acknowledgment, there is an automated procedure to redirect the token to drone  $i + 2$ , and so on. Additionally, any drone in the swarm will automatically reclaim the token if more than  $2(i + 1)$  s have passed since the last time it had the token. This mechanism preserves the functionality of the protocol even when the token-bearing drone falls outside of the communicable range or experiences a failure. The representation in Fig. 6E shows a simplified version of the protocol. After the token acquisition, a drone enters a brief listening period, spanning a random interval between 0-20 milliseconds to ascertain if another drone transmits during this time (i.e., has the token). Should the transmitting drone have a lower ID, the current drone discards the token. If not, it proceeds with the subsequent stages. This mechanism mitigates the situations where more drones have the token simultaneously. For example, if the drone carrying the token moves out of the swarm's radio range, another drone will claim the token. When the missing drone returns to the swarm, our protocol determines which drone keeps the token.

### Exploration algorithm

We introduce our lightweight exploration strategy used for the scope of this paper, which is formulated as a state machine and governs the behavior of individual robots. This strategy performs a pseudo-random exploration of a given environment without requiring a target destination. However, unlike other random exploration algorithms (6), this strategy prioritizes wall following and corner visiting (33), which encompass texture-rich areas favorable to loop closures. Regardless of the state, the goal of the exploration algorithm is to provide the body velocities (i.e.,  $v_x$ ,  $v_y$ ), and the heading angular rate  $\omega$ . Fig. 5A illustrates the three conditions of the state machine, where each robot starts in the "Cruise" mode, characterized by a cyclic execution of three steps. In the initial step, the algorithm adjusts the forward velocity  $v_x$  linearly, dependent on the frontal distance  $d$ , clipped with predefined lower and upper bounds  $v_{min}$  and  $v_{max}$ . Note that distance  $d$  is computed as the minimum value provided by the frontal depth sensor. The velocity curve is shown in Fig. 5B, where  $m$  represents the slope of the linear region. The second step verifies if there is a side obstacle within a lateral distance of  $2 d_{obj}$ . A proportional controller then adjusts  $v_y$  to position the drone at  $d_{obj}$  from the detected obstacle, as shown in Fig.5C. Fig.5D illustrates the final step of the "Cruise" state, where the robot checks for the presence of an object on either side. A line detector assesses if the depth measurements align with the expected readings from a flat surface. Based on the slope of the line, the system aligns the robot's orientation parallelly. If an object is detected on both sides, priority is given to the right. If an object is detected beyond the distance  $d_{obj}$  or not detected at all, the commanded angular rate  $\omega$  is set to 0. The first step of the "Cruise" state ensures smooth deceleration upon detecting a frontal obstacle, while subsequent steps facilitate effective wall following.

When a frontal obstacle is detected, and  $d$  becomes smaller than a threshold  $d_s$ , the system goes into the "Spinning" state. The direction of spinning is determined by evaluating  $d_L$  and  $d_R$  distances on the left and right, respectively. In the event of an obstacle detected to the left (i.e.,  $d_L < 2 d_{obj}$ ), the robot rotates clockwise (CW) as shown on the left side of Fig. 5E; conversely, if an obstacle is detected to the right, the robot rotates counter-clockwise (CCW). In scenarios where both sides are unobstructed, and the robot is situated at an intersection (i.e., Fig. 5E – right side), it counts how many other agents are on its left and right relative to its OX-axis (shown in grey) and turns towards the side with fewer robots. In the event of an equal number of robots on both sides, a random decision is made. When  $d$  becomes higher than  $d_s + \Delta_d$ , with  $\Delta_d = 0.3 m$ , a pathway ahead is again clear, and the system makes the transition back to the "Cruise" state.

If the mission is performed by one drone only, the system would only loop between "Cruise" and "Spinning" states. The transition to the "Caution" state can only be triggered by the interaction with another robot. Fig. 5F shows how each robot virtually splits the surroundings into four areas. If

there is an agent within the frontal (F) area at a distance lower than  $2 d_{obj}$ , i.e.,  $d_{UWB} < 2 d_{obj}$ , the system goes into the “Caution” state. In finding the presence of another agent within the frontal zone, the robot utilizes the received position estimates, while for determining proximity within a distance  $2 d_{obj}$ , it solely relies on UWB measurements. In the “Caution” state, the robot turns around  $180^\circ$ . During spinning, it also checks if an obstacle (i.e., wall or another agent) is located closer than a critical distance  $d_C$ , and sets  $v_x$  and  $v_y$  accordingly to push itself away from the obstacle, as illustrated in Fig. 5G. Note that the distances  $d_B, d_R$ , and  $d_L$  represent the minimum distances from the back, right, and left areas, respectively. When the robot completes spinning, it returns to the “Cruise” state.

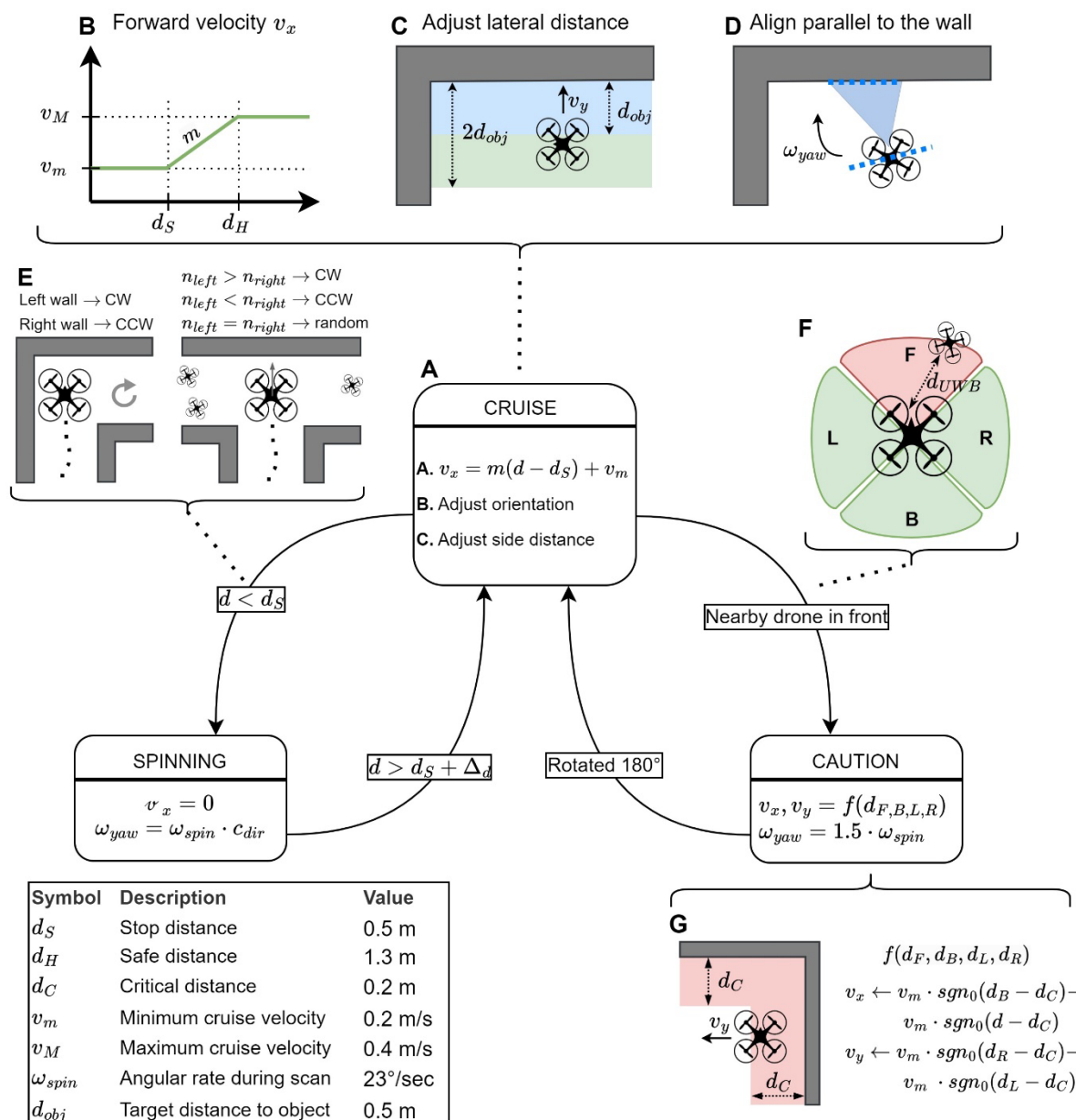


**Fig. 5. The exploration algorithm.** (A) The state machine of the exploration algorithm illustrating the behavior in each state and what conditions trigger transitions. (B) The velocity as a function of distance in the Cruise state. (C) An illustration of how the drone adjusts its side speed to keep a constant distance from a wall. (D) The figure shows how the drone sets the heading rate to keep itself parallel to a side wall. (E) The behavior of the drone once it reaches a corner or an intersection. (F) An illustration of the critical zone that indicates a possible collision with another drone. (G) The figure shows how the drone behaves in the Caution state, when it is close to a wall or obstacle.

## Hardware architecture

To demonstrate the flexibility and low computational demand of C-SLAM, all tests and results rely on the commercial platform Crazyflie 2.1 from Bitcraze, augmented with four plug-in circuit boards (i.e., decks). To maximize the flight time, we use the Tattu 350 mAh battery and BetaFPV motors. The COTS FlowDeck v2 provides the drone with improved odometry capabilities. It contains the PMW3901 optical flow sensor, which enables body-frame velocity estimation, while the VL53L1x sensor enables height estimation. The information provided by the sensors onboard the FlowDeck is fused with the information from the onboard inertial measurement unit (IMU) to calculate the odometry edges. The second COTS deck is the Loco Positioning deck, which enables UWB capabilities. Specifically for this work, we designed a custom deck that includes four depth sensors (i.e., the Quad ToF Deck) enabling the drone to acquire distance measurements from all directions. Lastly, we use an open-source deck featuring the GAP9 System-on-Chip (SoC) (34) from Greenwaves Technologies to extend the computational capabilities with a multi-core ultra-low power microcontroller that enables the execution of the C-SLAM algorithm. All the additional hardware that we employ is either commercially available or open-source, and the individual power consumption of each deck is provided in Fig. 7, along with an illustration of the fully integrated system.

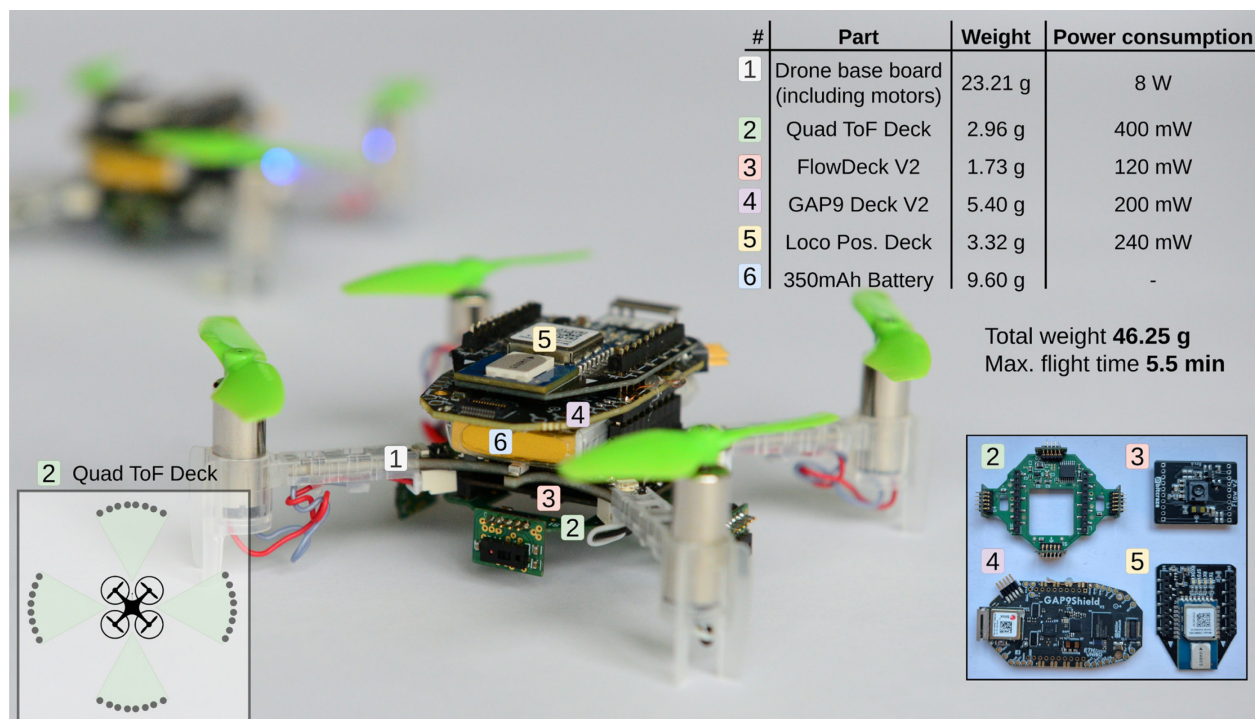


**Fig. 7. The hardware architecture.** The hardware platform used in our experiments, based on the Crazyflie v2 nano-UAV. Furthermore, the figure shows the modular deck stack, highlighting the weight and power consumption of each component.

## References and Notes

1. P. Arm, G. Waibel, J. Preisig, T. Tuna, R. Zhou, V. Bickel, G. Ligeza, T. Miki, F. Kehl, H. Kolvenbach, M. Hutter, Scientific exploration of challenging planetary analog environments with a team of legged robots. *Sci. Robot.* **8**, eade9548 (2023).
2. M. Dorigo, G. Theraulaz, V. Trianni, Reflections on the future of swarm robotics. *Sci. Robot.* **5**, eabe4385 (2020).

3. X. Zhou, X. Wen, Z. Wang, Y. Gao, H. Li, Q. Wang, T. Yang, H. Lu, Y. Cao, C. Xu, F. Gao, Swarm of micro flying robots in the wild. *Sci. Robot.* **7**, eabm5954 (2022).
4. J. A. Placed, J. Strader, H. Carrillo, N. Atanasov, V. Indelman, L. Carlone, J. A. Castellanos, A Survey on Active Simultaneous Localization and Mapping: State of the Art and New Frontiers. *IEEE Trans. Robot.* **39**, 1686–1705 (2023).
5. P.-Y. Lajoie, G. Beltrame, Swarm-SLAM: Sparse Decentralized Collaborative Simultaneous Localization and Mapping Framework for Multi-Robot Systems. *IEEE Robot. Autom. Lett.* **9**, 475–482 (2024).
6. K. N. McGuire, C. De Wagter, K. Tuyls, H. J. Kappen, G. C. H. E. De Croon, Minimal navigation solution for a swarm of tiny flying robots to explore an unknown environment. *Sci. Robot.* **4**, eaaw9710 (2019).
7. E. Soria, F. Schiano, D. Floreano, Predictive control of aerial swarms in cluttered environments. *Nat Mach Intell* **3**, 545–554 (2021).
8. V. S. Varadharajan, D. St-Onge, B. Adams, G. Beltrame, Swarm Relays: Distributed Self-Healing Ground-and-Air Connectivity Chains. *IEEE Robot. Autom. Lett.* **5**, 5347–5354 (2020).
9. R. J. Amala Arokia Nathan, I. Kurmi, O. Bimber, Drone swarm strategy for the detection and tracking of occluded targets in complex environments. *Commun Eng* **2**, 55 (2023).
10. V. Kratky, A. Alcantara, J. Capitan, P. Stepan, M. Saska, A. Ollero, Autonomous Aerial Filming With Distributed Lighting by a Team of Unmanned Aerial Vehicles. *IEEE Robot. Autom. Lett.* **6**, 7580–7587 (2021).
11. Y. Tian, Y. Chang, L. Quang, A. Schang, C. Nieto-Granda, J. P. How, L. Carlone, “Resilient and Distributed Multi-Robot Visual SLAM: Datasets, Experiments, and Lessons Learned” in *2023 IEEE/RSJ International Conference on Intelligent Robots and Systems (IROS)* (IEEE, Detroit, MI, USA, 2023; <https://ieeexplore.ieee.org/document/10342377/>), pp. 11027–11034.
12. G. C. H. E. De Croon, J. J. G. Dupeyroux, S. B. Fuller, J. A. R. Marshall, Insect-inspired AI for autonomous robots. *Sci. Robot.* **7**, eabl6334 (2022).
13. X. Zhou, J. Zhu, H. Zhou, C. Xu, F. Gao, “EGO-Swarm: A Fully Autonomous and Decentralized Quadrotor Swarm System in Cluttered Environments” in *2021 IEEE International Conference on Robotics and Automation (ICRA)* (IEEE, Xi’an, China, 2021; <https://ieeexplore.ieee.org/document/9561902/>), pp. 4101–4107.
14. Y. Tian, Y. Chang, F. Herrera Arias, C. Nieto-Granda, J. P. How, L. Carlone, Kimera-Multi: Robust, Distributed, Dense Metric-Semantic SLAM for Multi-Robot Systems. *IEEE Trans. Robot.* **38**, 2022–2038 (2022).
15. P.-Y. Lajoie, B. Ramtoula, Y. Chang, L. Carlone, G. Beltrame, DOOR-SLAM: Distributed, Online, and Outlier Resilient SLAM for Robotic Teams. *IEEE Robot. Autom. Lett.* **5**, 1656–1663 (2020).
16. P. E. Dupont, B. J. Nelson, M. Goldfarb, B. Hannaford, A. Menciassi, M. K. O’Malley, N. Simaan, P. Valdastri, G.-Z. Yang, A decade retrospective of medical robotics research from 2010 to 2020. *Sci. Robot.* **6**, eabi8017 (2021).
17. V. Iyer, A. Najafi, J. James, S. Fuller, S. Gollakota, Wireless steerable vision for live insects and insect-scale robots. *Sci. Robot.* **5**, eabb0839 (2020).
18. A. Grau, M. Indri, L. Lo Bello, T. Sauter, Robots in Industry: The Past, Present, and Future of a Growing Collaboration With Humans. *EEE Ind. Electron. Mag.* **15**, 50–61 (2021).
19. H. Müller, V. Niculescu, T. Polonelli, M. Magno, L. Benini, Robust and Efficient Depth-Based Obstacle Avoidance for Autonomous Miniaturized UAVs. *IEEE Trans. Robot.* **39**, 4935–4951 (2023).
20. M. S. Talamali, A. Saha, J. A. R. Marshall, A. Reina, When less is more: Robot swarms adapt better to changes with constrained communication. *Sci. Robot.* **6**, eabf1416 (2021).



21. F. Berlinger, M. Gauci, R. Nagpal, Implicit coordination for 3D underwater collective behaviors in a fish-inspired robot swarm. *Sci. Robot.* **6**, eabd8668 (2021).
22. A. Rosinol, M. Abate, Y. Chang, L. Carlone, “Kimera: an Open-Source Library for Real-Time Metric-Semantic Localization and Mapping” in *2020 IEEE International Conference on Robotics and Automation (ICRA)* (IEEE, Paris, France, 2020; <https://ieeexplore.ieee.org/document/9196885/>), pp. 1689–1696.
23. N. Baumann, E. Ghignone, J. Kühne, N. Bastuck, J. Becker, N. Imholz, T. Kränzlin, T. Y. Lim, M. Lötscher, L. Schwarzenbach, L. Tognoni, C. Vogt, A. Carron, M. Magno, ForzaETH Race Stack -- Scaled Autonomous Head-to-Head Racing on Fully Commercial off-the-Shelf Hardware. doi: 10.48550/ARXIV.2403.11784 (2024).
24. P. Huang, L. Zeng, X. Chen, L. Huang, Z. Zhou, S. Yu, Edge Robotics: Edge-Computing-Accelerated Multirobot Simultaneous Localization and Mapping. *IEEE Internet Things J.* **9**, 14087–14102 (2022).
25. M. A. Jamshed, K. Ali, Q. H. Abbasi, M. A. Imran, M. Ur-Rehman, Challenges, Applications, and Future of Wireless Sensors in Internet of Things: A Review. *IEEE Sensors J.* **22**, 5482–5494 (2022).
26. I. Vizzo, T. Guadagnino, B. Mersch, L. Wiesmann, J. Behley, C. Stachniss, KISS-ICP: In Defense of Point-to-Point ICP – Simple, Accurate, and Robust Registration If Done the Right Way. *IEEE Robot. Autom. Lett.* **8**, 1029–1036 (2023).
27. S. Fuller, Z. Yu, Y. P. Talwekar, A gyroscope-free visual-inertial flight control and wind sensing system for 10-mg robots. *Sci. Robot.* **7**, eabq8184 (2022).
28. S. Zhong, Y. Qi, Z. Chen, J. Wu, H. Chen, M. Liu, DCL-SLAM: A Distributed Collaborative LiDAR SLAM Framework for a Robotic Swarm. *IEEE Sensors J.* **24**, 4786–4797 (2024).
29. V. Niculescu, T. Polonelli, M. Magno, L. Benini, NanoSLAM: Enabling Fully Onboard SLAM for Tiny Robots. *IEEE Internet Things J.* **11**, 13584–13607 (2024).
30. Y. Song, A. Romero, M. Müller, V. Koltun, D. Scaramuzza, Reaching the limit in autonomous racing: Optimal control versus reinforcement learning. *Sci. Robot.* **8**, eadg1462 (2023).
31. D. Schindler, V. Niculescu, T. Polonelli, D. Palossi, L. Benini, M. Magno, “A Relative Infrastructure-less Localization Algorithm for Decentralized and Autonomous Swarm Formation” in *2023 IEEE/RSJ International Conference on Intelligent Robots and Systems (IROS)* (IEEE, Detroit, MI, USA, 2023; <https://ieeexplore.ieee.org/document/10342168/>), pp. 5288–5295.
32. F. Shan, J. Zeng, Z. Li, J. Luo, W. Wu, “Ultra-Wideband Swarm Ranging” in *IEEE INFOCOM 2021 - IEEE Conference on Computer Communications* (IEEE, Vancouver, BC, Canada, 2021; <https://ieeexplore.ieee.org/document/9488717/>), pp. 1–10.
33. B. P. Duisterhof, S. Li, J. Burgues, V. J. Reddi, G. C. H. E. De Croon, “Sniffy Bug: A Fully Autonomous Swarm of Gas-Seeking Nano Quadcopters in Cluttered Environments” in *2021 IEEE/RSJ International Conference on Intelligent Robots and Systems (IROS)* (IEEE, Prague, Czech Republic, 2021; <https://ieeexplore.ieee.org/document/9636217/>), pp. 9099–9106.
34. D. Rossi, F. Conti, M. Eggiman, A. D. Mauro, G. Tagliavini, S. Mach, M. Guermandi, A. Pullini, I. Loi, J. Chen, E. Flamand, L. Benini, Vega: A Ten-Core SoC for IoT Endnodes With DNN Acceleration and Cognitive Wake-Up From MRAM-Based State-Retentive Sleep Mode. *IEEE J. Solid-State Circuits* **57**, 127–139 (2022).

**Acknowledgments:** Authors thank Davide Plozza for his support during field tests. The GAP9 Deck V2 is designed by Victor Javier Kartsch Morinigo and Hanna Müller with the support of Greenwaves Technologies.

**Funding:** This work is supported in part by BRAINSEE project (#8003528831) funded by Armasuisse Science and Technology of the Swiss Confederation. Moreover, it is also partially supported by the ESA – Open Space Innovation Platform (OSIP) under ID: I-2023-03429.